

Co-pyrolysis of sewage sludge and grape dreg to produce efficient and low-cost biochar for methylene blue removal: adsorption performance and characteristics

Meng Mei^{a,b}, Jingxin Liu^{a,b}, Teng Wang^{a,b}, Si Chen^{a,b}, Damin Liu^a, Jinping Li^{a,b,*}

^aSchool of Environmental Engineering, Wuhan Textile University, Wuhan 430073, China, email: lijinpings@wtu.edu.cn (J. Li)

^bEngineering Research Centre for Clean Production of Textile Dyeing and Printing, Ministry of Education, Wuhan Textile University, Wuhan 430073, China

Received 16 June 2021; Accepted 17 December 2021

ABSTRACT

The feedstock has great effect on the property of biochar. In this work, grape dreg was first used as a carbon additive for sewage sludge to prepare co-pyrolyzed biochar adsorbent to remove methylene blue (MB) from aqueous solution. The yield and absorption capacity of biochar were greatly affected by the addition amount of grape dreg. The co-pyrolyzed biochar possessed high surface area and abundant functional groups. The adsorption process was well described by pseudo-second-order kinetic and Langmuir isotherm models. The thermodynamic analysis indicated the spontaneous and endothermic adsorption of MB. The maximum adsorption capacity were 30.98, 29.74 and 31.45 mg/g at 20°C, 30°C and 40°C, respectively. The adsorption mechanism was involved in pore filling, hydrogen bonding, electrostatic binding, ion-exchange and π - π stacking interactions. It can be concluded that the biochar co-pyrolyzed from sewage sludge and grape dreg has good potential for MB removal from aqueous sample.

Keywords: Biochar adsorbent; Co-pyrolysis; Sewage sludge; Grape dreg; Methylene blue

1. Introduction

Sewage sludge (SS) is the final residue from wastewater treatment cycles. Since an increasing number of wastewater treatment plants are constructed and operated, the generation of SS is growing year by year [1]. After the major wastewater problem solved, the management of SS becomes a great challenge owing to its massive bulk and the abundant toxic elements containing [2]. Generally, ocean dumping, incineration, landfill and agricultural application are the mostly used routes for SS disposal [3]. The ocean dumping way is simple and cost-effective, and has been adopted for many years. However, dumping SS at sea is almost banned at present because of the bad effect on marine ecosystem [4]. Although SS contains plentiful nutrients

(e.g., nitrogen and phosphorus) that needed by crops, the presence of hazardous heavy metals, pathogenic organisms and refractory organics narrows its use as fertilizers in agricultural cultivation [5]. Similarly, SS incineration and landfill can generate unwanted emissions into water, soil and air [4]. Considering the increasing public and political focus on the environmental protection, the conventional SS handling ways are seen more and more critical in the future. Therefore, the researchers' interest has switched to develop both safer and more effective treatment method for SS.

The pyrolysis disposal of SS is a thermal decomposition process under inert atmosphere, during which the solid waste can transform into liquid bio-oil, pyrolytic gas

* Corresponding author.

and solid char [6], and it is believed to be an economical and environmentally friendly measure for its significance in minimizing the volume of wastes and stabilizing the dangerous components [7]. After pyrolysis, the environmental risk of SS gets reduced, and more importantly, value-added products can be obtained, one of which is the attractive biochar. SS-derived biochar has the merits of effectiveness, low cost as well as abundant feedstock, and has drawn much attention in many research fields. One of attractive applications is as good alternative sorbents for adsorption in environmental remediation field. Compared to other methods such as precipitation, ion-exchange, membrane separation and photocatalysis [8,9], adsorption has stood out for its easier operability, more convenience and environmental-friendliness on the removal of pollutants [10,11]. The adsorbent is the core of adsorption method as it determines the cost and efficiency. The SS contains multifarious organic matters and it is viewed as prominent precursor to prepare biochar adsorbent. However, the intrinsic features of SS like high ash and low carbon content may result in the poor physicochemical characteristics of biochar in terms of porosity, specific surface area and reactive groups, which is not conducive to obtain satisfactory adsorbents [12,13]. Proper modifications are usually needed to improve the adsorption ability of SS-based biochar. Currently, there are primarily two modification ideas: activation and decoration. The former aims to develop porous structure and improve specific surface area by employing highly etching reagents such as acid/alkali solution [14,15], while the latter concentrates on enhancing surface activity of biochar by introducing dopant atoms [16–18] or grafting functional groups [19–21] to the carbon skeleton.

There is no doubt that the property of biochar is closely dominated by the type of feedstock [22]. On this view, it may be a feasible approach to boost the adsorption capacity of biochar by adjusting the nature of SS. It was reported that increasing the carbon content of SS by using some additives was beneficial to improve the physicochemical properties of biochar. For example, coal was used to blend with SS and the char with a surface area of 91.07 m²/g was obtained. This value was much higher than that of sole SS [23]. Compared with coal, agroforestry biomasses are a category of cheap, rich and renewable natural carbon source. Thus, they can be served as eco-friendly carbon additives for SS pyrolysis treatment. Up to now, various types of biomasses such as rice straw [24], rice husk [25], cotton stalks [26] and hazelnut shell [27] have been mixed and co-pyrolyzed with SS. Results indicated that the addition of carbon-rich biomass materials replenished the carbon content of SS and facilitated the improvements in mechanical and physicochemical characteristics of SS-based biochar [25,28]. By this way, the use of chemical modification reagents aimed at increasing the property and adsorbability of biochar could be significantly reduced. Furthermore, a number of researches pointed out that the utilization of biomass helped to promote the pyrolysis and, reduce the emissions of undesired gases and decrease the toxicity of harmful matters existing in the SS [24,28,29]. Therefore, it has been recognized that the co-pyrolyzed biochar as adsorbent is more suitable and reliable than pure SS-based biochar [12]. However, in previous researches,

much attention has been paid to the behaviors and characteristics of co-pyrolysis process [30,31], more efforts are needed to be made on the development and application of co-pyrolyzed biochar for pollutant detoxification.

Grape is the most consumed fruit in worldwide wine processing industry. It is said that about 70 million tons of wine grape are harvested and used to make wine every year [32]. Grape dreg (GD), the major solid wastes during wine production, is generated in large amounts. This kind of biomass is basically non-poisonous and possesses high content of organic matter [33]. The co-pyrolysis of GD with SS is an efficient way to promote waste utilization, and at the same time produce valuable adsorbent. However, there have been no reports on this regard. In present study, GD was blended with SS to prepared a co-pyrolyzed biochar. The influence of GD content was evaluated by the yield and the iodine absorption value of biochar. The physicochemical characteristics including apparent morphology, specific surface area, pore structure and functional groups of the biochar were analyzed. Subsequently, the co-pyrolyzed biochar was employed as an effective and low-cost adsorbent to remove methylene blue (MB) in aqueous sample. The batch adsorption experiments were conducted to investigate the effect of key parameters on removal process. Meanwhile, integrated with model analyzing, the sorption kinetic, isotherm and thermodynamic characteristics of MB on biochar were elucidated in detail.

2. Experimental

2.1. Reagents and materials

The dehydrated SS was sampled from an urban municipal wastewater treatment plant in Wuhan, China. GD came from the wine brewing laboratory of Wuhan Textile University. All feedstocks were firstly oven-dried at 105°C to constant weight, then grinded and screened through a 20-mesh sieve. The powder samples were stored in a desiccator for subsequent use. The general properties including moisture, organic matter and ash contents, pH values and elemental compositions of SS and GD were investigated. The MB and Na₂CO₃ of analytical quality were supplied by Sinopharm Chemical Reagent Co., Ltd., (Shanghai, China). Deionized water was used in all studies.

2.2. Preparation of co-pyrolyzed biochar

Firstly, the crushed GD and SS were homogeneously mixed at a mass ratio of 0:1, 0.5:1, 1:1, process 2:1, respectively. Next, the activator Na₂CO₃ with a mass ratio of 3:1 to the blends was added, and followed by a proper amount of water. The mixture was fully stirred and impregnated for 24 h under room temperature, and then dried at 105°C. The above carbon precursor was transferred to a porcelain crucible and pyrolyzed in a tubular furnace at a heating rate of 10°C/min under N₂ atmosphere (100 mL/min). The pyrolysis process was maintained at 400°C for 60 min. Afterwards, the product was collected and washed by 3 mol/L HCl solution. Then, the biochar was separated using a filter paper and washed with deionized water to neutral pH. After oven-dried at 105°C, the biochar was

milled to 200 mesh to obtain the adsorbent. The biochar co-pyrolyzed from SS and GD was indicated by SGB. The yield of biochar was obtained by the following formula [34]:

$$\text{Yield (wt.\%)} = \frac{\text{weight of biochar}}{\text{weight of raw materials}} \quad (1)$$

2.3. Characterizations

The iodine absorption values were measured according to the PRC National Standard (GB/T 12496.8-2015) to illustrate the adsorption ability of SGB prepared with different GD/SS mass ratio. The surface morphologies and functional groups of dried SS and SGB were analyzed by scanning electron microscopy (SEM, JSM-7001F, JEOL) and Fourier-transform infrared spectrometer (FTIR, VERTEX 70, Bruker), respectively. The Brunauer–Emmett–Teller (BET) surface area, porosity and pore volume were determined thorough N_2 adsorption–desorption experiment performed on the Micromeritic TriStar II 3020.

2.4. Adsorption experiments

Bath adsorption experiments were conducted to investigate the adsorption performance of SGB for MB at different initial pH, contact time, adsorbate concentration and adsorbent dosage. Fresh MB sample solutions were prepared by dissolving MB in deionized water in each sorption. For all tests, the predetermined amount of adsorbent was added into a 100 mL conical flask containing 50 mL MB solution, and then the bottle was sealed and placed in a thermostatic water bath oscillator with a shaking speed of 120 rpm at 30°C for adsorption. After a given time, the solid and liquid were centrifuged at 4,000 rpm for 10 min, the supernatant was withdrawn and filtered through a 0.45 μm syringe filter. The concentration of residual MB in the liquid was determined using a UV-Vis spectrophotometer (UV-5500PC) at the wavelength of 662 nm. According to Eqs. (2) and (3) below, the removal rate and adsorption capacity of MB were calculated.

$$\text{Removal rate (\%)} = \frac{C_0 - C_e}{C_0} \times 100 \quad (2)$$

$$Q_e = \frac{C_0 - C_e}{M} \times V \quad (3)$$

where C_0 (mg/L) and C_e (mg/L) represent the initial concentration and equilibrium concentration of MB, respectively; Q_e (mg/g) indicates the amount of MB adsorbed by per gram of SGB; V (L) is the volume of sample solution and M (g) is the weight of SGB.

The adsorption behaviors of MB onto SGB were explored by fitting the obtained results to typical adsorption models. As for kinetic study, the pseudo-first-order, pseudo-second-order and intraparticle diffusion models were employed, which are expressed as Eqs. (4)–(6) [8].

Pseudo-first-order:

$$\ln(Q_e - Q_t) = \ln Q_e - K_1 t \quad (4)$$

Pseudo-second-order:

$$\frac{t}{Q_t} = \frac{1}{K_2 Q_e^2} + \frac{t}{Q_e} \quad (5)$$

Intraparticle diffusion:

$$Q_t = K_{3-i} t^{0.5} + C_i \quad (6)$$

where Q_e (mg/g) and Q_t (mg/g) represent the absorption capacity at equilibrium point and time t (min), respectively; K_1 (min^{-1}), K_2 ($\text{g}/(\text{mg min})$), K_{3-i} ($\text{mg}/(\text{g min}^{1/2})$) are the pseudo-first-order, pseudo-second-order and intraparticle diffusion adsorption rate constants, respectively; C_i (mg/g) is the parameter related to the thickness of boundary layer.

As for the study of adsorption isotherms, Langmuir and Freundlich models described as Eqs. (7) and (8) were used [21].

Langmuir isotherm:

$$\frac{C_e}{Q_e} = \frac{1}{K_L Q_{\max}} + \frac{C_e}{Q_{\max}} \quad (7)$$

Freundlich isotherm:

$$\ln Q_e = \ln K_F + \frac{1}{n} \ln C_e \quad (8)$$

where C_e (mg/L) and Q_e (mg/g) stand for the concentration and adsorption capacity of MB at equilibrium point, respectively; whereas Q_{\max} (mg/g) is the maximum adsorption capacity; K_L (L/mg) and K_F ($(\text{mg}^{(1-1/n)} \text{L}^{1/n})/\text{g}$) are the constants of Langmuir model and Freundlich model, respectively, and n denotes the index related to adsorption capacity and intensity.

In addition, the thermodynamic study was carried out, from which the changes of energy (ΔG , kJ/mol), adsorption enthalpy (ΔH , kJ/mol) and adsorption entropy (ΔS , kJ/(K mol)) in adsorption process were calculated. The formulas are described as Eqs. (9) and (10) [35].

$$\ln K = \frac{\Delta S}{R} - \frac{\Delta H}{RT} \quad (9)$$

$$\Delta G = -RT \ln K \quad (10)$$

where R indicates the universal gas constant, the value is 8.314 J/(K mol); T (K) is the absolute temperature; K (dimensionless) represents the thermodynamic equilibrium constant, and was calculated as illustrated in literature [35].

3. Results and discussion

3.1. Addition amount of GD

Table 1 presents the basic properties of SS and GD. It was found that the SS had a neutral pH while GD was acidic, and both of them were of high moisture content. It is noticeable that the organic compounds and C element containing in GD were 81.76% and 48.21%, respectively, which were much higher than those in SS. On the contrary,

Table 1
General properties of SS and GD

Sample	SS	GD
pH	6.7	4.5
Moisture (wt.%)	88.20	67.52
Organic matter ^a (wt.%)	52.47	81.76
Ash ^a (wt.%)	47.53	18.24
C ^a (wt.%)	18.79	48.21
H ^a (wt.%)	3.24	5.54
O ^a (wt.%)	18.61	42.88
N ^a (wt.%)	2.97	1.98
S ^a (wt.%)	1.23	0.49

^aMeasured on a dry basis.

the ash content of GD was much lower than that of SS. The results indicated that GD could function as a good carbon additive for SS. In this study, different amount of GD was mixed with SS to acquire the precursor for biochar preparation. As depicted in Fig. 1, with the GD/SS mass ratio increasing from 0 to 2, the biochar yield exhibited a slightly declining trend. Whereas the adsorption ability was enhanced, which can be confirmed from the increasing iodine number from 124.61 to 458.91 mg/g. This was attributed to the higher carbon and lower ash contents of GD than those of SS. Briefly, the addition of GD increased the total carbon content of feedstock, meaning that more organic compounds might decompose for pore formation during the pyrolysis process [12]. Hence, less biochar was obtained because of more mass loss, and meanwhile, the adsorption performance was improved owing to the richer micropores and actives sites [36–38]. In addition, the natural pore structure of GB biomass made it easier for activator to enter into the inner of SS, which favored the formation of micropores as well. In present work, to maximize the utilization of SS and ensure the removal efficiency at the same time, the GD/SS mass ratio at 2 was used to prepare SGB.

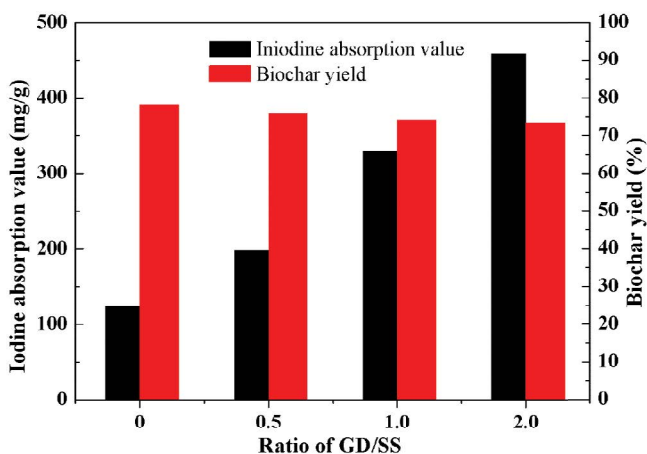


Fig. 1. Effect of GD percentage on iodine absorption value and yield of biochar.

3.2. Materials characterization

The SEM analysis was carried out to observe the morphological changes before and after carbonization. As can be seen from Fig. 2a, the dried SS owned dense and compact surface with limited porosity. For SGB, by contrast, coarser and fluffier structure could be noticed (Fig. 2b), which implied that it possessed excellent porosity [36]. The differences in surface morphologies were further verified by N₂ adsorption–desorption experiment. Results indicated that SGB showed a high BET surface area (425.72 m²/g) with large total pore volume (0.231 cm³/g), which were much larger than those of dried SS (13.87 m²/g and 0.070 cm³/g, respectively). These data were in good agreement with SEM results. To further understand the chemical groups on SGB surface, the FTIR spectrum in the range of 400–4,000 cm⁻¹ was curve fitted (Fig. 2c). The adsorption band at 3,615 cm⁻¹ was ascribed to the stretching vibration of O–H, peaks at 2,921 cm⁻¹ and 2,849 cm⁻¹ corresponded the adsorption of CH₃ and CH₂ functional groups, respectively [34,39]. The existence of C=O group could be confirmed by the peak at 1,705 cm⁻¹ [40]. The adsorption peaks appeared at 1,609, 1,030 and 795 cm⁻¹ were related to aromatic C=C, C–O and C–H groups, respectively [41]. The results confirmed the diversity of functional groups on the surface of SGB, which played important roles during adsorption process.

3.3. Effects of experimental conditions on adsorption process

The adsorption performance of SGB under different conditions such as sample pH, adsorbent dosage, initial MB concentration and contact time was thoroughly evaluated. pH is a non-negligible factor because it has prominent impact on the existing forms and stabilities of both adsorbent and adsorbate [42]. Considering the actual pH of wastewater and practical maneuverability, the pH values of MB solution in the present study were adjusted to 5.51, 6.25, 7.62, 8.41 and 9.25 with 0.1 mol/L HCl and 0.1 mol/L NaOH. Fig. 3a shows that the removal rate and adsorption capacity of MB were basically stable at all examined pH values, indicating the good stability and applicability of SGB. Thus, the pH was not adjusted in the following studies.

Fig. 3b describes the effect of SGB dosage on the removal of MB. The removal rate of MB kept increasing with the dosage of MB varying from 0.05 to 0.20 g. Initially, less than half of MB was removed at 0.05 g dosage. When more adsorbent was used, the binding sites for adsorption increased and near about 86.3% of MB could be removed by 0.10 g of SGB. While further increasing the amount of SGB, there was a little improvement in the removal rate of MB. However, with the increase of SGB dosage, the adsorption capacity declined rapidly. This was because the high dosage of SGB provides more available sites for adsorption, resulting in the decreased utilization of active sites on per unit mass of SGB [43]. Hence, from the viewpoint of cost-saving, the dosage of SGB at 0.10 g was adopted for further study.

The effect of initial MB concentration on adsorption efficiency was conducted by varying the concentration of MB from 10 to 130 mg/L. The adsorption capacity was improved by enhancing the initial concentration of MB. It was due to that the higher concentration produced

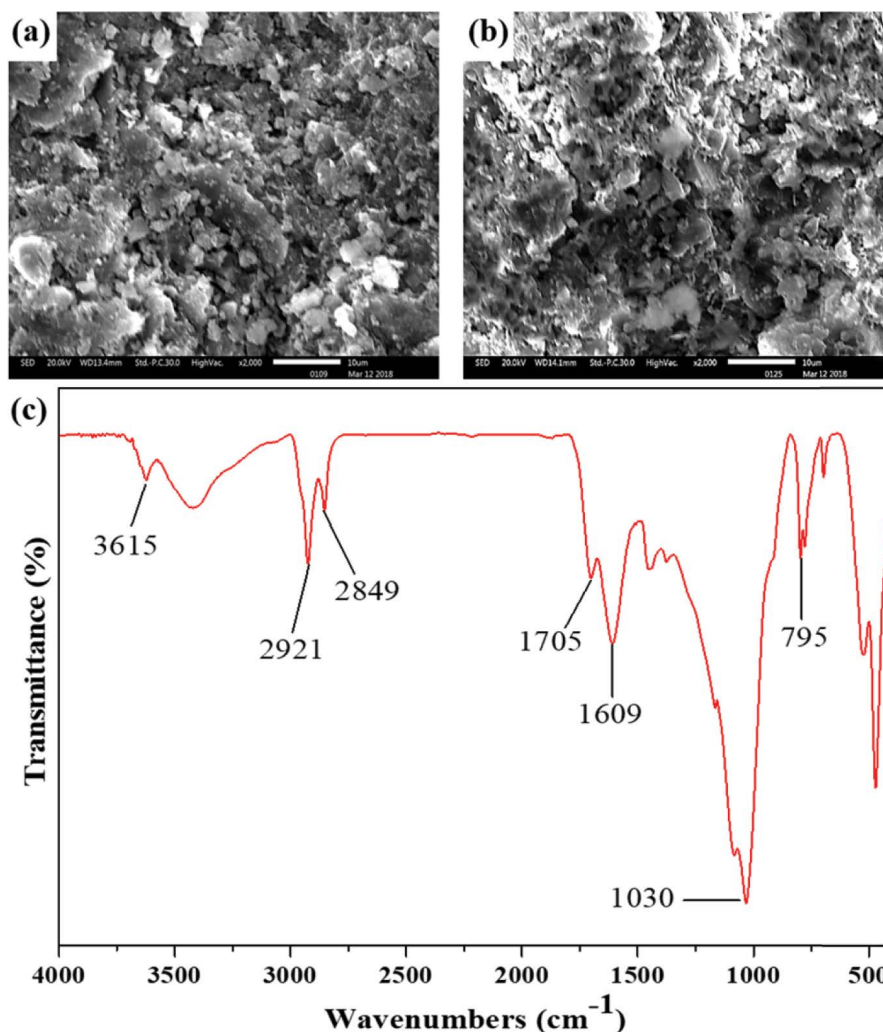


Fig. 2. SEM images of (a) dried SS, (b) SGB, and (c) the FTIR spectrum of SGB.

stronger mass transfer driving force and more MB were transferred to the SGB surface. However, since the number of adsorption sites was limited by the adsorbent amount, the removal rate of MB gradually decreased with the increase of concentration, just as depicted in Fig. 3c [44].

The study on contact time is strongly recommended because it reflects the speed and efficiency of an adsorption system. The removal rate and adsorption capacity of MB at different contact time are shown in Fig. 3d. It can be found that the adsorption of MB was very fast at first 40 min. This was attributed to the abundant active sites available at early stage. Thereafter, very little enhancement in adsorption rate was achieved. It was observed that adsorption equilibrium could be reached within 120 min.

3.4. Adsorption characteristics and mechanisms

3.4.1. Kinetics

In order to better understand the mechanism of the adsorption process, the pseudo-first-order, pseudo-second-order and intraparticle diffusion models were used to

analyze the data. Fig. 4a–c display the fitting lines of kinetic study obtained at 30, 50 and 70 mg/L of MB, respectively. Various kinetic parameters for different models were calculated and concluded in Table 2. It can be found that the pseudo-second-order model showed a remarkable linearity with R^2 values all very close to 1 at three concentrations, while the pseudo-first-order model has lower R^2 values in the range of 0.9154–0.9591. The results demonstrated that the pseudo-second-order model was much more appropriate to describe the MB binding on SGB. Therefore, the removal of MB was mainly affected by chemical interaction [40].

Furthermore, intraparticle diffusion model was adopted to recognize the diffusion mechanism and possible rate controlling step. As shown in Fig. 4c, the plots of Q_t vs. $t^{0.5}$ fitted at different concentrations were divided into two linear portions. None of them went through the zero point, indicating the adsorption rate was determined by multiple steps, and not merely by the diffusion process [45]. The multi-linearity of fitting lines manifested that there were two stages for MB adsorption. The first was the external mass transfer stage from 0 to 60 min, resulting from the diffusion of MB from solution to the exterior boundary of

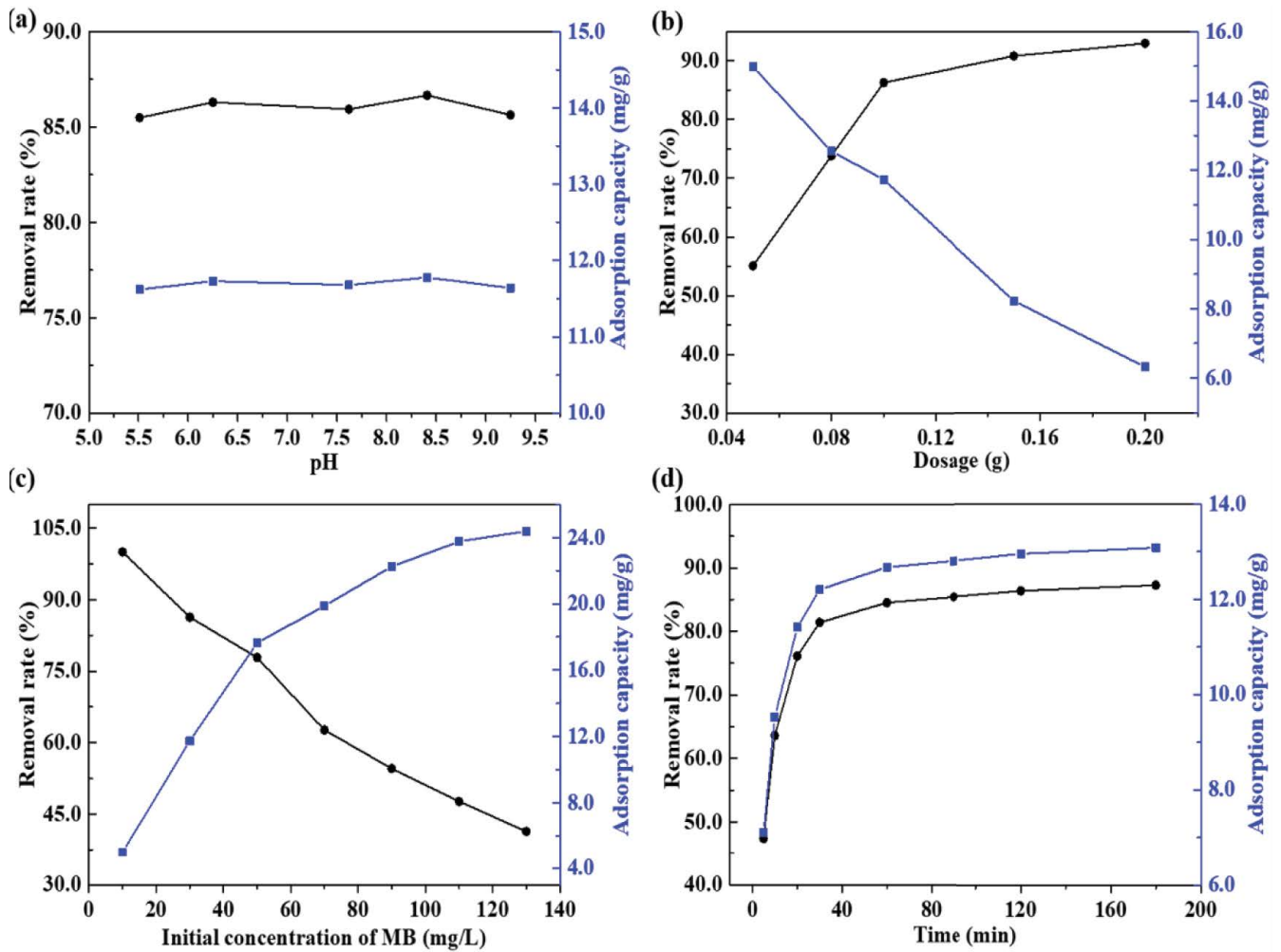


Fig. 3. Effects of (a) initial pH, (b) SGB dosage, (c) MB concentration and (d) contact time on removal performance.

Table 2
Results of kinetic study for the adsorption of MB by SGB

Kinetic model	Parameter	Values at different initial concentration (mg/L)		
		30	50	70
Pseudo-first-order	K_1	0.025	0.023	0.022
	Q_e	3.35	8.51	9.93
	R^2	0.9154	0.9591	0.9553
Pseudo-second-order	K_2	0.021	0.007	0.005
	Q_e	13.34	20.28	22.66
	R^2	0.9999	0.9999	0.9999
Intraparticle diffusion	K_{3-1}	2.812	2.812	3.225
	C_1	4.129	1.852	1.247
	R_1^2	0.9243	0.9622	0.9530
	K_{3-2}	0.106	0.357	0.451
	C_2	11.751	15.025	16.025
	R_2^2	0.8832	0.9027	0.8942

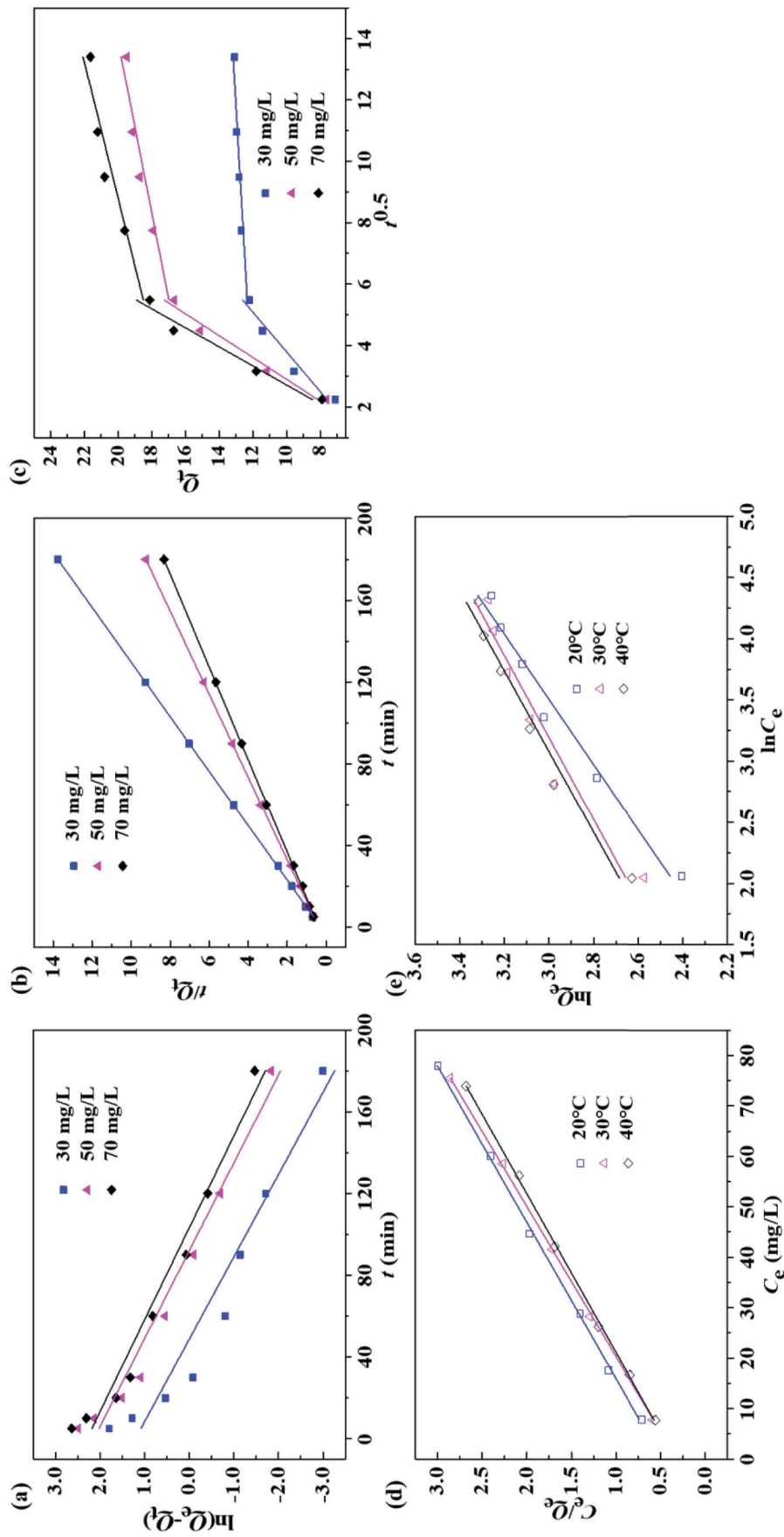


Fig. 4. Adsorption kinetics for MB adsorption on SGB with (a) pseudo-first-order, (b) pseudo-second-order and (c) intraparticle diffusion models, and adsorption isotherms with (d) Langmuir and (e) Freundlich models.

SGB. The second corresponded to the intraparticle diffusion stage from 60 to 180 min. This was attributed to the further diffusion from the external surface to the internal pore structure of SGB. Table 2 displays the parameters of two stages. It is clearly found that the values of K_{3-1} were much higher than those of K_{3-2} , indicating that MB molecules were adsorbed quickly on the surface of SGB because abundant active sites were available at initial contact, and over time, the diffusion rate of MB inside the SGB slowed down due to the decreasing number of active sites [46]. The above results revealed that the adsorption of MB on SGB was a multi-phase diffusion process involving surface adsorption and intraparticle diffusion.

3.4.2. Isotherms

In this study, two well-known models of Langmuir and Freundlich isotherms were used for further investigation of adsorption characteristics. The former is based on the assumption that all adsorption sites are equivalent and a monolayer adsorption occurs on a homogeneous surface, while the latter is more utilized when the surface of adsorbent is heterogeneous and multi-layer adsorption occurs [47]. All analyzed results are summarized in Fig. 4c–d and Table 3. Apparently, the Langmuir isotherm model could better fit the adsorption process of MB on SGB because it

provided higher correlation coefficients (0.9988–0.9994) than the Freundlich isotherm model (0.9196–0.9688) at three studied temperatures. This indicated that the adsorption process belonged to a monolayer adsorption, and MB molecules were preferred to be adsorbed by the identical sites on the homogeneous surface of SGB [48]. The n values calculated from Freundlich model were between 1 and 10, indicating the prone and favorable adsorption of MB on SGB [46]. Besides, the potential maximum adsorption capacity of SGB for MB was evaluated based on Langmuir model. The maximum adsorption capacity for MB were 30.98, 29.74 and 31.45 mg/g at 20°C, 30°C and 40°C, respectively. Hence, it was believed that the SGB had satisfactory affinity towards MB and could be a potential adsorbent for MB decontamination from aqueous sample. The comparison of SGB with other previously reported biochar adsorbents was conducted. As shown in Table 4, it was found that the pyrolysis temperature for SGB was much lower than most of other studies. However, the SGB exhibited a higher surface area as well as superior removal capacity for MB than other materials.

3.4.3. Thermodynamics

Thermodynamic study was conducted at 20°C, 30°C and 40°C to better evaluated the effect of temperature

Table 3
Isotherm and thermodynamic parameters for MB adsorption on SGB

Temperature (°C)	Langmuir isotherm			Freundlich isotherm			ΔG	ΔH	ΔS
	K_L	Q_{\max}	R^2	K_F	n	R^2			
20	0.066	30.98	0.9985	5.397	2.668	0.9688	-24.27		
30	0.106	29.74	0.9994	7.757	3.356	0.9196	-26.27	14.14	0.132
40	0.097	31.45	0.9988	7.911	3.304	0.9588	-26.91		

Table 4
Comparison results of present study with other reports for MB adsorption

Feedstocks	Pyrolysis conditions	Surface area (m ² /g)	Dosage (g/L)	Q_{\max} (mg/g)/T (°C)	References
Mixed municipal discarded material (paper, cardboard, food scraps and garden waste)	300°C, 12 h	NM ^a	5	7.254/30	[49]
Corn cob	500°C, 2 h	655.79	5	15.80/25	[50]
Pine wood	500°C, 2 h	198.03	10	3.99/25	[51]
Pig manure	500°C, 2 h	346.97	10	16.30/25	[51]
Cardboard	500°C, 2 h	310.82	10	1.66/25	[51]
Switch grass	600°C, 1 h	255.8	2	37.6/NM ^a	[52]
Municipal sludge	550°C, 2 h	25	6	24.1/25	[53]
Municipal solid wastes (60% paper, 25% yard wastes and 15% textiles)	683°C, 53 min	NM ^a	2	21.83/30	[54]
Pulp and paper sludge	750°C, 2 h	174	5	33/NM ^a	[55]
Sewage sludge/tea waste	300°C, 2 h	NM ^a	10	12.58/25	[56]
Sewage sludge/grape dreg	400°C, 1 h	425.72	2	30.98/20	This study

^aNM: Not mentioned.

on adsorption process. The related parameters including ΔG , ΔH and ΔS were calculated and listed in Table 3. In all cases, negative ΔG values were obtained, confirming the spontaneous nature of MB adsorption onto SGB. Furthermore, with the temperature increasing from 20°C to 40°C, the ΔG values decreased from -24.27 to -26.91 kJ/mol, revealing that the MB could be adsorbed by SGB more easily and efficiently at a relatively higher temperature. Thus, it could be inferred that the adsorption reaction was endothermic, and this character was further verified by the positive values of ΔH . The positive ΔS value indicated the randomness increase at the solution/sorbent interface [57].

3.4.4. Adsorption mechanism of SGB for MB

From the above discussion, it can be concluded that the adsorption of MB on SGB was a multi-step process, involving the MB transfer from liquid phase to the solid phase, and the diffusion of MB into the inner surface and pores of SGB. Both physical adsorption and chemical bonding contributed to the removal of MB. The physical adsorption was attributed to the high surface area and proper pore size for pore filling [56]. However, according to the results of kinetic study, chemisorption was the governing mechanism of adsorption. This was mainly attributed to the abundant functional groups on the surface of SGB, especially the oxygen-containing functional groups including O–H, C=O and C–O that have been confirmed by FTIR. The potential importance of this type of group in pollutant decontamination have been announced by many reports [58,59]. It was said that oxygen-containing groups could lead to a negatively charged surface of biochar, which was beneficial for the capture of cationic MB through electrostatic interaction [60]. Oxygen and nitrogen atoms are well-known receptors for hydrogen bonds. The existence of oxygen on the surface of SGB facilitated the formation of hydrogen bonds between biochar and the amine groups of MB molecules [61]. Furthermore, oxygen-containing group such as $-\text{COOH}$ was the good producer for cationic exchange interaction [56]. Thus, it was believed that hydrogen bonding, electrostatic binding and ion-exchange interactions were all participated in the removal of MB [61,62]. Meanwhile, the graphitic structure of biochar generated during the pyrolysis process could bind with the aromatic structure of MB through π - π stacking interaction, which also contributed to the adsorption [44]. The possible adsorption mechanism of MB on SGB is illustrated in Fig. 5.

4. Conclusions

In present work, GD was co-pyrolyzed with SS for the first time to obtain a low-cost biochar adsorbent SGB for MB removal. Results showed that the addition of GD led to a significant increase in adsorption ability of biochar. The prepared SGB was rich in functional groups and exhibited a high specific surface area of 425.72 m²/g. It was found that the adsorption of MB by SGB was a spontaneous and endothermic process, which could be described by pseudo-second-order kinetic and Langmuir isotherm models. The maximum adsorption capacity for MB were determined to

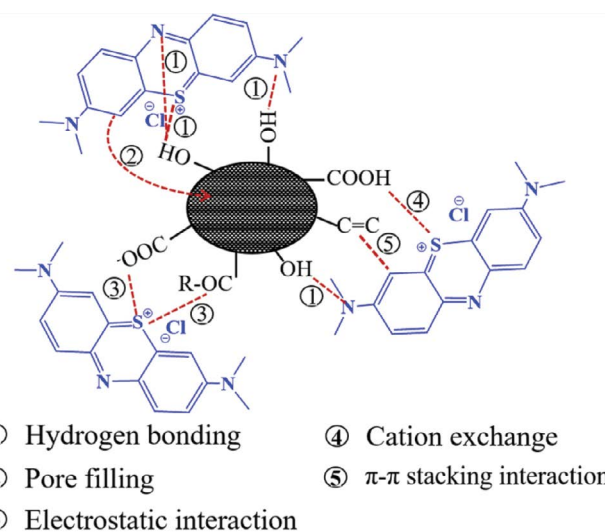


Fig. 5. Possible adsorption mechanism of MB onto SGB.

be 30.98, 29.74 and 31.45 mg/g at 20°C, 30°C and 40°C, respectively, revealing that the developed SGB could be served as an efficient and low-cost adsorbent to remove MB.

Acknowledgement

This study was financially supported by Science and Technology Research Project of Education Department of Hubei Province (No. B2021092) and the Engineering Research Centre for Clean Production of Textile Dyeing and Printing, Ministry of Education. The authors would also like to thank all reviewers for commenting on this paper.

References

- [1] R.R.Z. Tarpani, C. Alfonsín, A. Hospido, A. Azapagic, Life cycle environmental impacts of sewage sludge treatment methods for resource recovery considering ecotoxicity of heavy metals and pharmaceutical and personal care products, *J. Environ. Manage.*, 260 (2020) 109643.
- [2] S. Ozdemir, S.M. Turp, N. Oz, Simultaneous dry-sorption of heavy metals by porous adsorbents during sludge composting, *Environ. Eng. Res.*, 25 (2020) 258–265.
- [3] M.M. Mian, G.J. Liu, B. Fu, Conversion of sewage sludge into environmental catalyst and microbial fuel cell electrode material: a review, *Sci. Total Environ.*, 666 (2019) 525–539.
- [4] A. Zaker, Z. Chen, X.L. Wang, Q. Zhang, Microwave-assisted pyrolysis of sewage sludge: a review, *Fuel Process. Technol.*, 187 (2019) 84–104.
- [5] J.H. Seo, N. Kim, M. Park, S. Lee, S. Yeon, D. Park, Evaluation of metal removal performance of rod-type biosorbent prepared from sewage-sludge, *Environ. Eng. Res.*, 25 (2020) 700–706.
- [6] V. Fristak, M. Pipiska, G. Soja, Pyrolysis treatment of sewage sludge: a promising way to produce phosphorus fertilizer, *J. Clean. Prod.*, 172 (2018) 1772–1778.
- [7] J.W. Jin, Y.N. Li, J.Y. Zhang, S.C. Wu, Y.C. Cao, P. Liang, J. Zhang, M.H. Wong, M.Y. Wang, S.D. Shan, P. Christie, Influence of pyrolysis temperature on properties and environmental safety of heavy metals in biochars derived from municipal sewage sludge, *J. Hazard. Mater.*, 320 (2016) 417–426.
- [8] G. Sharma, D.D. Dionysiou, S. Sharma, A. Kumar, A.H. Al-Muhtaseb, M. Naushad, F.J. Stadler, Highly efficient Sr/Ce/activated carbon bimetallic nanocomposite for photoinduced degradation of rhodamine B, *Catal. Today*, 335 (2019) 437–451.

- [9] G. Sharma, A. Kumar, M. Naushad, B. Thakur, D.N. Vo, B. Gao, A.A. Al-Kahtani, F.J. Stadler, Adsorptional-photocatalytic removal of fast sulphon black dye by using chitin-cl-poly(itaconic acid-co-acrylamide)/zirconium tungstate nano-composite hydrogel, *J. Hazard. Mater.*, 416 (2021) 125714.
- [10] G. Sharma, M. Naushad, D. Pathania, A. Mittal, G.E. El-desoky, Modification of Hibiscus cannabinus fiber by graft copolymerization: application for dye removal, *Desal. Water Treat.*, 54 (2015) 3114–3121.
- [11] T.Y. Li, Y.Z. He, X.X. Peng, Efficient removal of tetrabromobisphenol A (TBBPA) using sewage sludge-derived biochar: adsorptive effect and mechanism, *Chemosphere*, 251 (2020) 126370.
- [12] Q.L. Liang, Y.C. Liu, M.Y. Chen, L.L. Ma, B. Yang, L.L. Li, Q. Liu, Optimized preparation of activated carbon from coconut shell and municipal sludge, *Mater. Chem. Phys.*, 241 (2020) 122327.
- [13] E. Agrafioti, G. Bouras, D. Kalderis, E. Diamadopoulos, Biochar production by sewage sludge pyrolysis, *J. Anal. Appl. Pyrolysis*, 101 (2013) 72–78.
- [14] L. Tang, J.F. Yu, Y. Pang, G.M. Zeng, Y.C. Deng, J.J. Wang, X.Y. Ren, S.J. Ye, B. Peng, H.P. Feng, Sustainable efficient adsorbent: alkali-acid modified magnetic biochar derived from sewage sludge for aqueous organic contaminant removal, *Chem. Eng. J.*, 336 (2018) 160–169.
- [15] L.Y. Li, X.D. Gong, O. Abida, Waste-to-resources: exploratory surface modification of sludge-based activated carbon by nitric acid for heavy metal adsorption, *Waste Manage.*, 87 (2019) 375–386.
- [16] J. Wei, Y.T. Liu, J. Li, Y.H. Zhu, H. Yu, Y.Z. Peng, Adsorption and co-adsorption of tetracycline and doxycycline by one-step synthesized iron loaded sludge biochar, *Chemosphere*, 236 (2019) 124254.
- [17] Y.F. Ma, P. Li, L. Yang, L. Wu, L.Y. He, F. Gao, X.B. Qi, Z.L. Zhang, Iron/zinc and phosphoric acid modified sludge biochar as an efficient adsorbent for fluoroquinolones antibiotics removal, *Ecotoxicol. Environ. Saf.*, 196 (2020) 110550.
- [18] W.R. Hu, Y. Xie, S. Lu, T.H. Xie, Y.K. Zhang, Y.B. Wang, One-step synthesis of nitrogen-doped sludge carbon as a bifunctional material for the adsorption and catalytic oxidation of organic pollutants, *Sci. Total Environ.*, 680 (2019) 51–60.
- [19] X. Huang, D. Wei, X.W. Zhang, D.W. Fan, X. Sun, B. Du, Q. Wei, Synthesis of amino-functionalized magnetic aerobic granular sludge-biochar for Pb(II) removal: adsorption performance and mechanism studies, *Sci. Total Environ.*, 685 (2019) 681–689.
- [20] X.R. Jing, Y.Y. Wang, W.J. Liu, Y.K. Wang, H. Jiang, Enhanced adsorption performance of tetracycline in aqueous solutions by methanol-modified biochar, *Chem. Eng. J.*, 248 (2014) 168–174.
- [21] S.Q. Tang, N.N. Shao, C.M. Zheng, F. Yan, Z.T. Zhang, Amino-functionalized sewage sludge-derived biochar as sustainable efficient adsorbent for Cu(II) removal, *Waste Manage.*, 90 (2019) 17–28.
- [22] A. Ahmad, N. Khan, B.S. Giri, P. Chowdhary, P. Chaturvedi, Removal of methylene blue dye using rice husk, cow dung and sludge biochar: characterization, application, and kinetic studies, *Bioresour. Technol.*, 306 (2020) 123202.
- [23] P. Xiao, L. Xu, X.D. Wang, Z.B. Chang, Co-pyrolysis characteristics of coal and sludge blends using thermogravimetric analysis, *Environ. Prog. Sustainable Energy*, 34 (2015) 1780–1789.
- [24] Q. Dong, S.P. Zhang, B. Wu, M. Pi, Y.Q. Xiong, H.Y. Zhang, Co-pyrolysis of sewage sludge and rice straw: thermal behavior and char characteristic evaluations, *Energy Fuels*, 34 (2020) 607–615.
- [25] T. Wang, Y.C. Chen, J.P. Li, Y.J. Xue, J.X. Liu, M. Mei, H.B. Hou, S. Chen, Co-pyrolysis behavior of sewage sludge and rice husk by TG-MS and residue analysis, *J. Clean. Prod.*, 250 (2020) 119557.
- [26] Z.P. Wang, X.Q. Shu, H.N. Zhu, L.K. Xie, S.H. Cheng, Y.X. Zhang, Characteristics of biochars prepared by co-pyrolysis of sewage sludge and cotton stalk intended for use as soil amendments, *Environ. Technol.*, 41 (2018) 1347–1357.
- [27] B. Zhao, X.Y. Xu, S.C. Xu, X. Chen, H.B. Li, F.Q. Zeng, Surface characteristics and potential ecological risk evaluation of heavy metals in the bio-char produced by co-pyrolysis from municipal sewage sludge and hazelnut shell with zinc chloride, *Bioresour. Technol.*, 243 (2017) 375–383.
- [28] S.H. Deng, H.Z. Tan, X.B. Wang, F.X. Yang, R.J. Cao, Z. Wang, R.H. Ruan, Investigation on the fast co-pyrolysis of sewage sludge with biomass and the combustion reactivity of residual char, *Bioresour. Technol.*, 239 (2017) 302–310.
- [29] Z.P. Wang, L.K. Xie, K. Liu, J. Wang, H.N. Zhu, Q. Song, X.Q. Shu, Co-pyrolysis of sewage sludge and cotton stalks, *Waste Manage.*, 89 (2019) 430–438.
- [30] X.B. Wang, S.H. Deng, H.Z. Tan, A. Adeosun, M. Vujanovic, F.X. Yang, N. Duic, Synergetic effect of sewage sludge and biomass co-pyrolysis: a combined study in thermogravimetric analyzer and a fixed bed reactor, *Energy Convers. Manage.*, 118 (2016) 399–405.
- [31] J.W. Jin, M.Y. Wang, Y.C. Cao, S.C. Wu, P. Liang, Y.N. Li, J.Y. Zhang, J. Zhang, M.H. Wong, S.D. Shan, P. Christie, Cumulative effects of bamboo sawdust addition on pyrolysis of sewage sludge: biochar properties and environmental risk from metals, *Bioresour. Technol.*, 228 (2017) 218–226.
- [32] B. Khiari, M. Jeguirim, Pyrolysis of grape marc from Tunisian wine industry: feedstock characterization, thermal degradation and kinetic analysis, *Energies*, 11 (2018) 730.
- [33] A. Ibn Ferjani, M. Jeguirim, S. Jellali, L. Limousy, C. Courson, H. Akroun, N. Thevenin, L. Ruidavets, A. Muller, S. Bennici, The use of exhausted grape marc to produce biofuels and biofertilizers: effect of pyrolysis temperatures on biochars properties, *Renewable Sustainable Energy Rev.*, 107 (2019) 425–433.
- [34] H.J. Huang, T. Yang, F.Y. Lai, G.Q. Wu, Co-pyrolysis of sewage sludge and sawdust/rice straw for the production of biochar, *J. Anal. Appl. Pyrolysis*, 125 (2017) 61–68.
- [35] J.H. Qu, Y.H. Yuan, Q.J. Meng, G.S. Zhang, F.X. Deng, L. Wang, Y. Tao, Z. Jiang, Y. Zhang, Simultaneously enhanced removal and stepwise recovery of atrazine and Pb(II) from water using β -cyclodextrin functionalized cellulose: characterization, adsorptive performance and mechanism exploration, *J. Hazard. Mater.*, 400 (2020) 123142.
- [36] Q.D. Chen, H. Liu, J. Ko, H.N. Wu, Q.Y. Xu, Structure characteristics of bio-char generated from co-pyrolysis of wooden waste and wet municipal sewage sludge, *Fuel Process. Technol.*, 183 (2019) 48–54.
- [37] Y.Q. Yi, G.Q. Tu, D.Y. Zhao, P.E. Tsang, Z.Q. Fang, Biomass waste components significantly influence the removal of Cr(VI) using magnetic biochar derived from four types of feedstocks and steel pickling waste liquor, *Chem. Eng. J.*, 360 (2019) 212–220.
- [38] W. Suliman, J.B. Harsh, N.I. Abu-Lail, A.M. Fortuna, I. Dallmeyer, M. Harcia-Perez, Influence of feedstock source and pyrolysis temperature on biochar bulk and surface properties, *Biomass Bioenergy*, 84 (2016) 37–48.
- [39] S. Saadat, E. Raei, N. Talebbeydokhti, Enhanced removal of phosphate from aqueous solutions using a modified sludge derived biochar: comparative study of various modifying cations and RSM based optimization of pyrolysis parameters, *J. Environ. Manage.*, 225 (2018) 75–83.
- [40] Q.Q. Yin, M.T. Liu, H.P. Ren, Biochar produced from the co-pyrolysis of sewage sludge and walnut shell for ammonium and phosphate adsorption from water, *J. Environ. Manage.*, 249 (2019) 109410.
- [41] J.W. Dai, X.F. Meng, Y.H. Zhang, Y.J. Huang, Effects of modification and magnetization of rice straw derived biochar on adsorption of tetracycline from water, *Bioresour. Technol.*, 311 (2020) 123455.
- [42] D.D. Sewu, P. Boakye, S.H. Woo, Highly efficient adsorption of cationic dye by biochar produced with Korean cabbage waste, *Bioresour. Technol.*, 224 (2017) 206–213.
- [43] Y. Zhang, M. Li, J.C. Li, Y.Y. Yang, X. Liu, Surface modified leaves with high efficiency for the removal of aqueous Cr(VI), *Appl. Surf. Sci.*, 484 (2019) 189–196.
- [44] M. Choudhary, R. Kumar, S. Neogi, Activated biochar derived from *Opuntia ficus-indica* for the efficient adsorption of malachite green dye, Cu²⁺ and Ni²⁺ from water, *J. Hazard. Mater.*, 392 (2020) 122441.

- [45] Y.T. Xu, J.X. Bao, X. Zhang, W.S. Li, Functionalized polyethersulfone nanofibrous membranes with ultra-high adsorption capacity for organic dyes by one-step electrospinning, *J. Colloid Interface Sci.*, 533 (2019) 526–538.
- [46] Z.U. Ahmad, L.G. Yao, J. Wang, D.D. Gang, F. Islam, Q.Y. Lian, M.E. Zappi, Neodymium embedded ordered mesoporous carbon (OMC) for enhanced adsorption of sunset yellow: characterizations, adsorption study and adsorption mechanism, *Chem. Eng. J.*, 359 (2019) 814–826.
- [47] F.A. Razmi, N. Ngadi, S. Wong, I.B. Inuwa, L.A. Opotu, Kinetics, thermodynamics, isotherm and regeneration analysis of chitosan modified pandan adsorbent, *J. Clean. Prod.*, 231 (2019) 98–109.
- [48] Y.F. Ma, M. Li, P. Li, L. Yang, L. Wu, F. Gao, X.B. Qi, Z.L. Zhang, Hydrothermal synthesis of magnetic sludge biochar for tetracycline and ciprofloxacin adsorptive removal, *Bioresour. Technol.*, 319 (2021) 124199.
- [49] J. Hoslett, H. Ghazal, N. Mohamad, H. Jouhara, Removal of methylene blue from aqueous solutions by biochar prepared from the pyrolysis of mixed municipal discarded material, *Sci. Total Environ.*, 714 (2020) 136832.
- [50] T. Suwunwong, N. Hussain, S. Chantrapromma, K. Phoungthong, Facile synthesis of corncob biochar via in-house modified pyrolysis for removal of methylene blue in wastewater, *Mater. Res. Express*, 7 (2020) 015518.
- [51] L. Lonappan, T. Rouissi, R.K. Das, S.K. Brar, A.A. Ramirez, M. Verma, R.Y. Surampalli, J.R. Valero, Adsorption of methylene blue on biochar microparticles derived from different waste materials, *Waste Manage.*, 49 (2016) 537–544.
- [52] J.H. Park, J.J. Wang, Y.L. Meng, Z. Wei, R.D. DeLaune, D.C. Seo, Adsorption/desorption behavior of cationic and anionic dyes by biochars prepared at normal and high pyrolysis temperatures, *Colloids Surf., A*, 572 (2019) 274–282.
- [53] S.S. Fan, Y. Wang, Z. Wang, J. Tang, J. Tang, X.D. Li, Removal of methylene blue from aqueous solution by sewage sludge-derived biochar: adsorption kinetics, equilibrium, thermodynamics and mechanism, *J. Environ. Chem. Eng.*, 5 (2017) 601–611.
- [54] D.A.G. Sumalinog, S.C. Capareda, M.D.G. de Luna, Evaluation of the effectiveness and mechanisms of acetaminophen and methylene blue dye adsorption on activated biochar derived from municipal solid wastes, *J. Environ. Manage.*, 210 (2018) 255–262.
- [55] N. Chaukura, E.C. Murimba, W. Gwenzi, Sorptive removal of methylene blue from simulated wastewater using biochars derived from pulp and paper sludge, *Environ. Technol. Innov.*, 8 (2017) 132–140.
- [56] S.S. Fan, J. Tang, Y. Wang, H. Li, H. Zhang, J. Tang, Z. Wang, X.D. Li, Biochar prepared from co-pyrolysis of municipal sewage sludge and tea waste for the adsorption of methylene blue from aqueous solutions: kinetics, isotherm, thermodynamic and mechanism, *J. Mol. Liq.*, 220 (2016) 432–441.
- [57] G.D. Degermenci, N. Degermenci, V. Ayvaoglu, E. Durmaz, D. Cakir, E. Akan, Adsorption of reactive dyes on lignocellulosic waste: characterization, equilibrium, kinetic and thermodynamic studies, *J. Clean. Prod.*, 225 (2019) 1220–1229.
- [58] G. Sharma, B. Thakur, A. Kumar, S. Sharma, M. Naushad, F.J. Stadler, Atrazine removal using chitin-*cl*-poly(acrylamide-co-itaconic acid) nanohydrogel: Isotherms and pH responsive nature, *Carbohydr. Polym.*, 241 (2020) 116258.
- [59] Y.Q. Yang, N. Chen, C.P. Feng, M. Li, Y. Gao, Chromium removal using a magnetic corncob biochar/polypyrrole composite by adsorption combined with reduction: reaction pathway and contribution degree, *Colloids Surf., A*, 556 (2018) 201–209.
- [60] Y. Zhu, B.J. Yi, Q.X. Yuan, Y.L. Wu, M. Wang, S.P. Yan, Removal of methylene blue from aqueous solution by cattle manure-derived low temperature biochar, *RSC Adv.*, 8 (2018) 19917–19929.
- [61] S. Liu, J.H. Li, S. Xu, M.Z. Wang, Y.C. Zhang, X.H. Xue, A modified method for enhancing adsorption capability of banana pseudostem biochar towards methylene blue at low temperature, *Bioresour. Technol.*, 282 (2019) 48–55.
- [62] B. Chen, H.N. Zhao, S.J. Chen, F.X. Long, B. Huang, B.Q. Yang, X.J. Pan, A magnetically recyclable chitosan composite adsorbent functionalized with EDTA for simultaneous capture of anionic dye and heavy metals in complex wastewater, *Chem. Eng. J.*, 356 (2019) 69–80.